

Liquid Chain Genesis by Collision of Two Laminar Jets

Vatsal Sanjay, Arup K. Das†

Department of Mechanical and Industrial Engineering, Indian Institute of Technology, Roorkee

(Received xx; revised xx; accepted xx)

Lorem ipsum dolor sit amet, consectetur adipiscing elit. Ut purus elit, vestibulum ut, placerat ac, adipiscing vitae, felis. Curabitur dictum gravida mauris. Nam arcu libero, nonummy eget, consectetur id, vulputate a, magna. Donec vehicula augue eu neque. Pellentesque habitant morbi tristique senectus et netus et malesuada fames ac turpis egestas. Mauris ut leo. Cras viverra metus rhoncus sem. Nulla et lectus vestibulum urna fringilla ultrices. Phasellus eu tellus sit amet tortor gravida placerat. Integer sapien est, iaculis in, pretium quis, viverra ac, nunc. Praesent eget sem vel leo ultrices bibendum. Aenean faucibus. Morbi dolor nulla, malesuada eu, pulvinar at, mollis ac, nulla. Curabitur auctor semper nulla. Donec varius orci eget risus. Duis nibh mi, congue eu, accumsan eleifend, sagittis quis, diam. Duis eget orci sit amet orci dignissim rutrum.

Key words:

1. Introduction

Interactions of liquid jets have invoked the curiosity of researchers with their ubiquitous presence, eminent even in the scientific artworks by Leonardo Da Vinci in the 16th century. Physics of different types of interactions related to liquid jets is classically summarized in a recent effort by Eggers & Villermaux (2008). One of these interactions is the collision between liquid jets, presented by Rayleigh (1879). Bush & Hasha (2004) introduced several regimes to characterize the different flow structures obtained from such collisions, working on the theory of liquid jet impingement given by Taylor (1960). At low velocities or narrow angles of impingement, jets may coalesce to form a unified one or bounce off due to presence of a thin film of air between them (Wadhwa *et al.* 2013). On increasing the flow rates, laminar jets may lead to formation of a stable liquid sheet bounded by a thick rim (Yang *et al.* 2014). Inertia and gravitational forces act to expand the liquid sheet formed but the action of surface tension puts a check and allows the sheet to converge, such that the successive collisions of the thick rims downstream of the flow result in formation of mutually orthogonal liquid sheets (Bush & Hasha 2004). Figure 1a illustrates this structure termed as the liquid chain with the complementary orthogonal sheets forming the different links. Alternatively, further increase in jet velocity, due to several instability modes, leads towards ejection of droplets from the liquid rim (Bremond & Villermaux 2006), fluid fishbones (Bush & Hasha 2004) and flapping sheet (Villermaux & Clanet 2002) associated with atomized drops (Ibrahim & Przekwas 1991). The stable chain regime is not just an idealization of the violent flapping, but also holds physical significance for the exploration of fundamental physics behind atomization. Moreover,

† Email address for correspondence: arupdias80@gmail.com

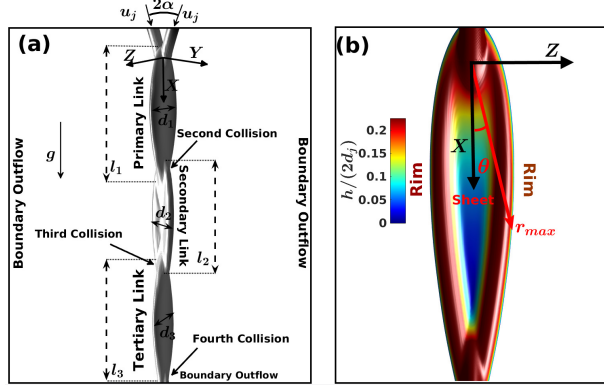


FIGURE 1. Formation of the liquid sheet by collision of laminar jets. (a) A schematic to illustrate different structural features and length scales. The mutually perpendicular sheets mark different links of the fluid chain structure. (b) The primary link structure colored based on half times the magnitude of the sheet thickness, non-dimensionalized with the jet diameter ($\frac{h}{2d_j}$).

these structures can be used as wall-free continuous reactors (Erni & Elabbadi 2013) and are often used as a canonical arrangement for generation of liquid sheets (Dombrowski & Fraser 1954).

Keeping this fascinating applications in mind, a range of experimental works can be found exploring the formation of stable liquid sheets using viscous jets (Choo & Kang 2001, 2002; Bush & Hasha 2004). Using Particle Image Velocimetry (PIV) technique, radial streamlines are observed near the point of impingement and the fluid parcels travel towards the periphery resulting in the formation of the thick rim due to fluid accumulation (Choo & Kang 2002; Bush & Hasha 2004). The rim is stable as long as the curvature force developed by surface tension provides the necessary centripetal acceleration as the fluid packets in the rim accelerate owing to loss in gravitational potential (Bremond & Villermaux 2006). On balancing the two, Taylor (1960) developed an expression for the sheet radius which has been found to describe the experimental results of Bush & Hasha (2004) reasonably well. Emphasis has been also given by Bush & Hasha (2004) for prediction of shapes of leaf like links forming chain structure. However, the model requires input from the experiments so as to close the system of differential equations. Isolated numerical efforts are also found describing different possible outcomes due to liquid jets interactions. As a part of their study, Chen *et al.* (2013) have shown formation of liquid chain using Finite Volume based Volume of Fluid (VOF) network. Recently, Da *et al.* (2016) also demonstrated formation of liquid chain using Boundary Element Method (BEM). But, their exhibition of chain like structure along with other physical jet related structures suffer from inviscid assumption.

Critical assessment of literature reveals that an in-depth study of fluid chain regime is still due which can explore fundamental physics behind formation of primary link and establish relation between successive diminishing links. Major challenge that lies in the prediction of chain like structure is the proper resolution of sheet (approximately 1/100th of jet diameter) between the rims, which are supposed to mingle once again for forming next link in mutually perpendicular plane. Figure 1b is presented to demonstrate the presence of a range of length scales in such a simplistic fluid link. In the present work, we attempt at study of an overall behavior of the fluid chain while focusing on the physics of flow for the primary link by analyzing the dimensional characteristics and velocity fields. Special attention is given to the second and third collisions, leading to the formation

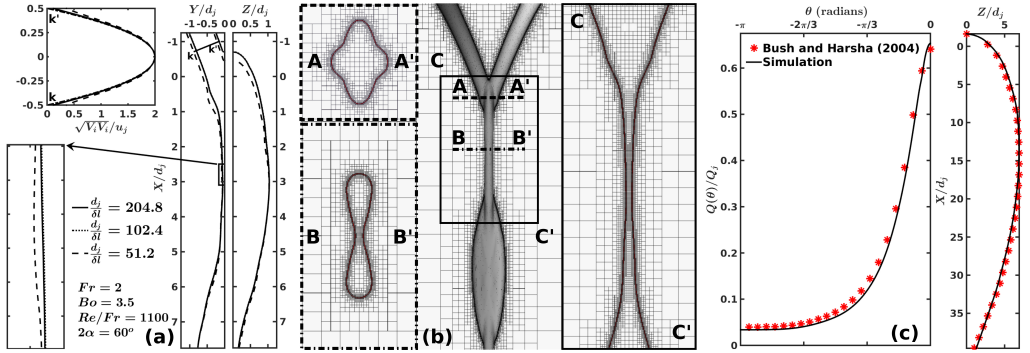


FIGURE 2. (a) Mesh Sensitivity Analysis for a representative chain structure with outer periphery and velocity profile near the inlet; (b) Representation of the Adaptive Mesh Refinement (AMR) technique at critical locations; (c) Numerical interface (left) and Liquid flux (right) superimposed with the respective experimental values obtained by Bush & Hasha (2004) to depict validation.

of the subsequent mutually orthogonal links and relate them from fundamental force balance. In the next section, the numerical framework employed in this work is briefly explained before reporting mesh sensitivity analysis and validation.

2. Numerical framework

Collision of liquid jets has been studied in three-dimensional finite volume framework. Open source, time-dependent, multi-fluid, Navier-Stokes solver, Gerris is used for the current study (Popinet 2003). The spatial discretization of the domain is undertaken using an octree based structured hierarchical grid system, locally refined near the interface. Conventional mass and momentum conservation equations for incompressible flow have been solved in presence of interface specific surface tension force ($\sigma\kappa$, where σ is the surface tension coefficient and κ denotes the curvature of the interface) and gravitational field (ρg). The interface tracking is undertaken using the Volume Of Fluid (VOF) approach using volume fraction of liquid, defined as $\Psi(x_i, t)$, at the spatial and temporal instance of x_i and t respectively. Therefore, the density and viscosity for the study can be described using Equation 2.1.

$$A(\Psi) = \Psi A_1 + (1 - \Psi) A_2 \quad \forall A \in \{\rho, \mu\} \quad (2.1)$$

The VOF approach is implemented in a two-step process of interface reconstruction (based on the values of Ψ and piecewise linear interface construction scheme, PLIC) along with geometric flux computation and interface advection, shown in Equation 2.2.

$$\frac{\partial \Psi}{\partial t} + \frac{\partial(\Psi V_i)}{\partial X_i} = 0 \quad (2.2)$$

Gerris uses second order accurate time discretization of momentum and continuity equations with time splitting algorithm as proposed by Chorin (1968), whereby an unconditionally stable corrector predictor time marching approach is adopted. A multi-grid solver is used for solution of the resulting pressure-velocity coupled Laplace equation. The advection term of the momentum equation ($V_k \frac{\partial V_i}{\partial X_k}$) is estimated using the Bell-Colella-Glaz second-order unsplit upwind scheme (Bell *et al.* 1989), which requires the restriction to be set up on the time step. Following Popinet (2009), time step has been determined to satisfy Courant-Friedrich-Lowy (CFL) stability criteria of less than unity. The details of solution procedure can be found in the works of Popinet (2003, 2009).

The computational domain is also illustrated in Figure 1a with parabolic inflow (average velocity, u_j) of jets (diameter, d_j and impingement angle, 2α) and boundary outflow elsewhere. From the works of Choo & Kang (2001), it can be easily shown that the thickness of liquid sheet follows $\frac{hr}{d_j^2} \sim 1$, for $2\alpha \in \{0, \pi/2\}$. Here, r is the radial direction originating from the collision point of the jets and h is the measurement of thickness of the film produced by jet collision. We maintained $\frac{d_j}{\delta l} \sim 10 \frac{r_{max}}{d_j}$ to choose minimum cell size (δl) and perform Grid Independence Study (GIS). The factor of 10 is included to have at least 10 grid points(Ling *et al.* 2015) across the smallest length scale for the structure to avoid breakage of sheet (Chen *et al.* 2013). To obtain continuous liquid film and well resolved phenomenon, δl is varied to match the above mentioned criteria. In one representative simulation, we show the effect of variation of δl , in Figure 2a, on sheet profile and velocity pattern of the jet. It can be observed that at $\frac{d_j}{\delta l} = 102.4$, well resolved film is obtained with acceptable computational cost ($\sim 50\%$ less than $\frac{d_j}{\delta l} = 204.8$). Mesh structure around different critical parts of the chain is shown in Figure 2b which establishes sufficiency of grid points even inside smallest thickness of the film. To check the accuracy of the developed mesh structure, results from simulations are compared (Figure 2c) with experimental observations of sheet profile reported by Bush & Hasha (2004). So as to get quantitative validation, variation of liquid volume flux inside the sheet is also plotted in Figure 2 along with Bush & Hasha (2004). In both the cases, matching between present numerical simulations and pioneering experimental result by Bush & Hasha (2004) provides confidence for numerical understanding of the phenomenon, in our work. Further, on performing non-dimensional analysis, it can be observed that Froude number $(Fr = \frac{u_j}{\sqrt{gd_j}})$, Bond number $(Bo = \frac{\rho gd_j^2}{\sigma})$ and ratio between Reynolds number and jet Froude number $(Re/Fr = \frac{\rho \sqrt{gd_j^3}}{\mu})$ govern the shape and sizes of different links in the fluid chain structure. In our next section, detailed effort has been presented to investigate formation of chain based on above non-dimensional numbers.

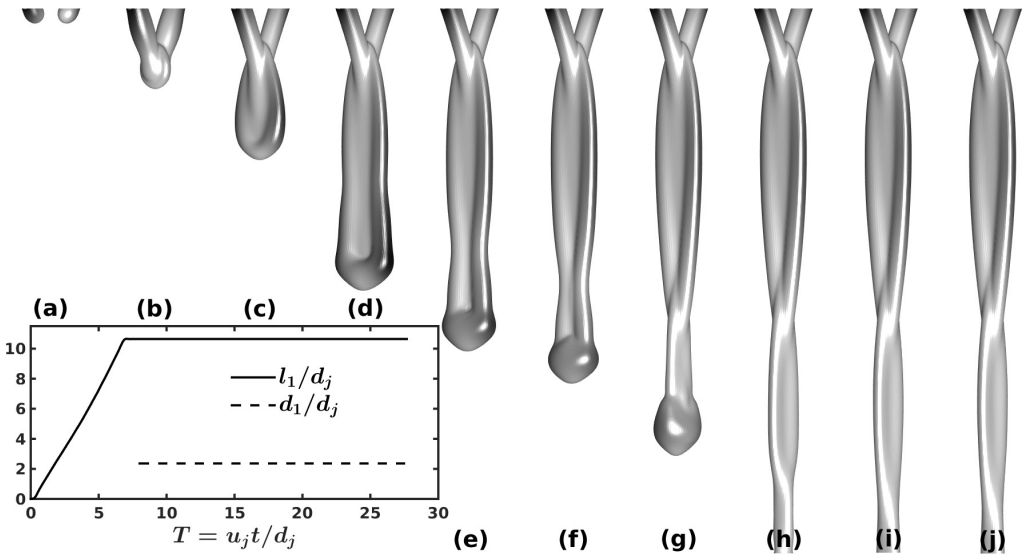


FIGURE 3. Transition to the steady state fluid-links chain formed by collision of laminar jets. The figure illustrates the transient period through the temporal advancement from (a) pre-collision symmetric jets to $T(\frac{u_j t}{d_j}) =$ (b) 1.5, (c) 4, (d) 5, (e) 5.5, (f) 6.5, (g) 8.5, (h) 16.5, (i) and (j) 20

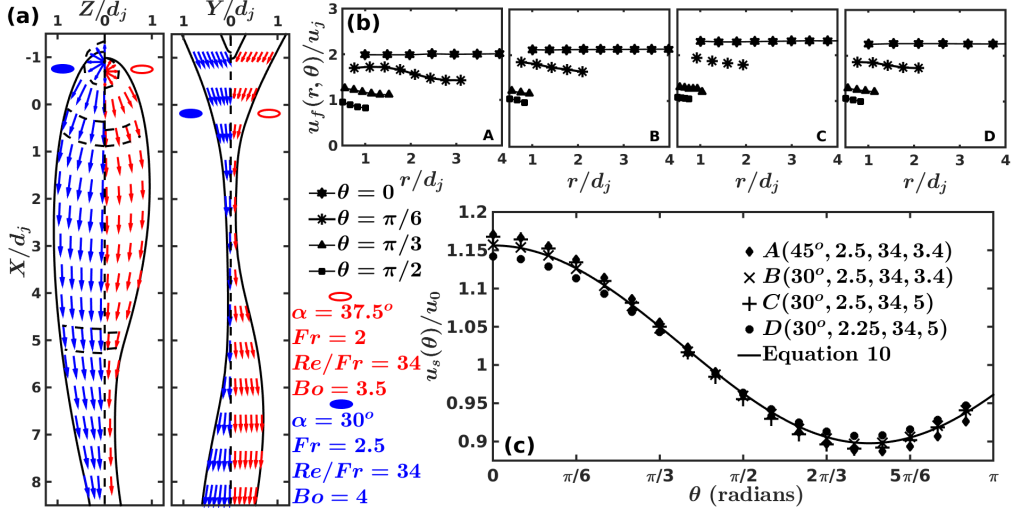


FIGURE 4. Flow kinematics of the fluid parcels inside the liquid sheet: (a) Velocity vector field for two representative cases with different flow and physical parameters, the vector field is radial near the stagnation point and then follows the self similar phase contour, (b) Variation of velocity in the radial direction for four representative cases with $(\alpha, Fr, Re/Fr, Bo)$: A($45^\circ, 2.5, 34, 3.4$), B($30^\circ, 2.5, 34, 3.4$), C($30^\circ, 2.5, 34, 5$) and D($30^\circ, 2.25, 34, 5$) and (c) Variation of the radially averaged sheet velocity (u_s), non-dimensionalized with the average sheet velocity (u_0) along the azimuthal direction in the sheet.

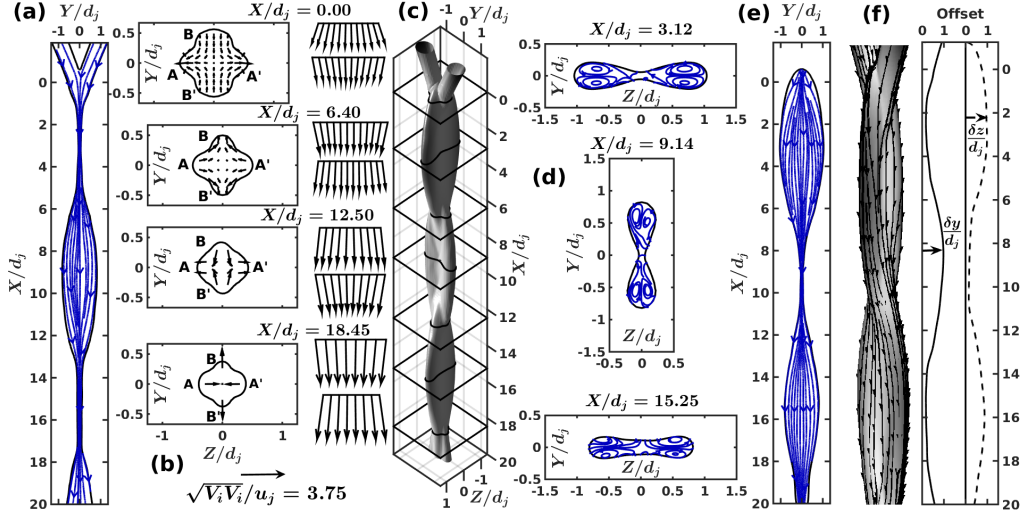


FIGURE 5. Flow kinematics of the fluid parcels inside the liquid sheet: (a) Velocity vector field for two representative cases with different flow and physical parameters, the vector field is radial near the stagnation point and then follows the self similar phase contour, (b) Variation of velocity in the radial direction for four representative cases with $(\alpha, Fr, Re/Fr, Bo)$: A($45^\circ, 2.5, 34, 3.4$), B($30^\circ, 2.5, 34, 3.4$), C($30^\circ, 2.5, 34, 5$) and D($30^\circ, 2.25, 34, 5$) and (c) Variation of the radially averaged sheet velocity (u_s), non-dimensionalized with the average sheet velocity (u_0) along the azimuthal direction in the sheet.

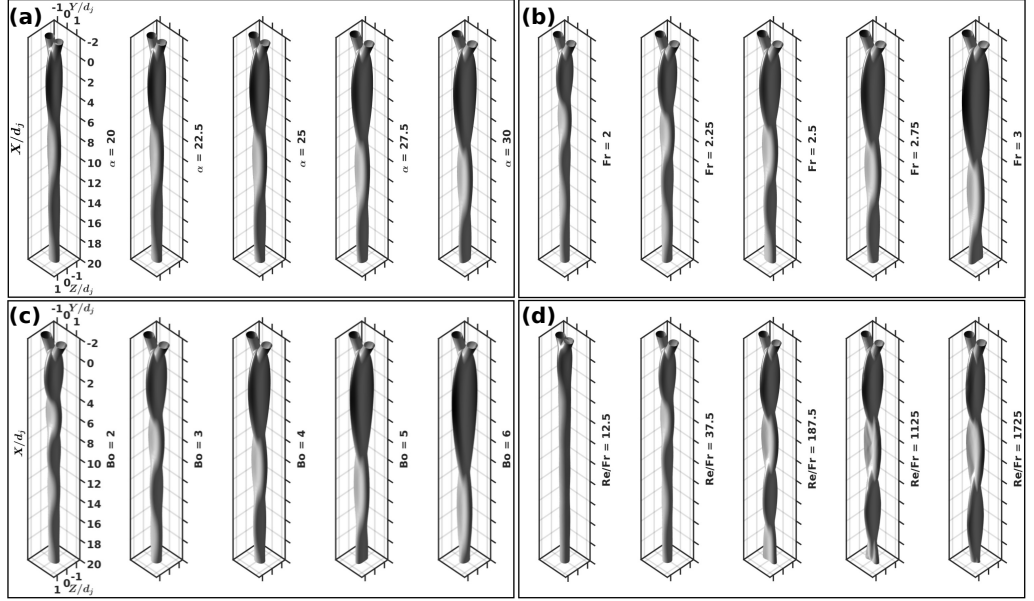


FIGURE 6. High fidelity numerical simulations of liquid jets collision to form chain structure for variation of (a) Re/Fr at $Fr = 2, Bo = 3.4, \alpha = 30$ (b) Fr at $Re/Fr = 34, Bo = 3.4, \alpha = 30$ (c) Bo at $Re/Fr = 34, Fr = 2.5, \alpha = 30$ and (d) α at $Re/Fr = 34, Fr = 2.5, Bo = 4.57$

	C_0	C_1	C_2	C_3	C_4
p_0	3.662	-0.082	-2.822	-1.504	-0.657
p_1	2.720	0.490	-1.231	-0.831	-0.290
p_2	0.353	1.146	0.437	0.074	0.029
p_3	0.512	0.592	0.800	-0.065	0.039

TABLE 1. Factors ($C_{m,n}$) involved in Equation ?? determined by regression analysis to get the coefficients p_n of Equation ??

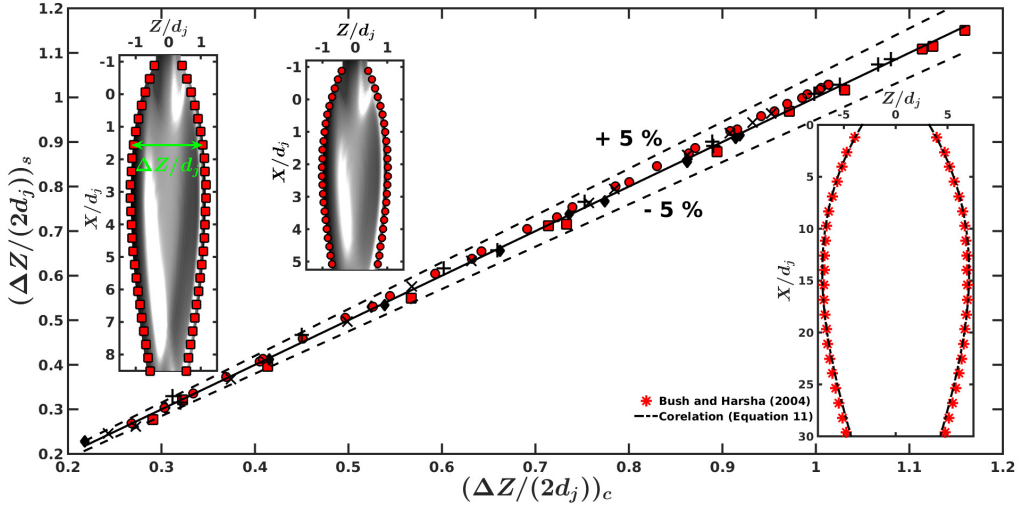


FIGURE 7. Comparison between the values of expansion of the sheet outer periphery ($\Delta Z(x)$) as obtained from correlations ($(\Delta Z/(2d_j))_c$) given in Equation ?? and from numerical simulations ($(\Delta Z/(2d_j))_s$) for different parametric variations of testing data with (symbol, α , Fr , Re/Fr , Bo) = (\blacksquare , 30° , 2.5, 34, 5); first inset figure from the left; (+, 30° , 2.5, 34, 4); (\blacklozenge , 30° , 2.5, 20, 2.3); (\times , 25° , 2.5, 34, 4.57) and (\bullet , 30° , 2.5, 20, 3.75); second inset figure from the left. In the last inset figure (from the left), comparison between the correlation model given in Equation ?? and experimental results of Bush & Hasha (2004) is provided.

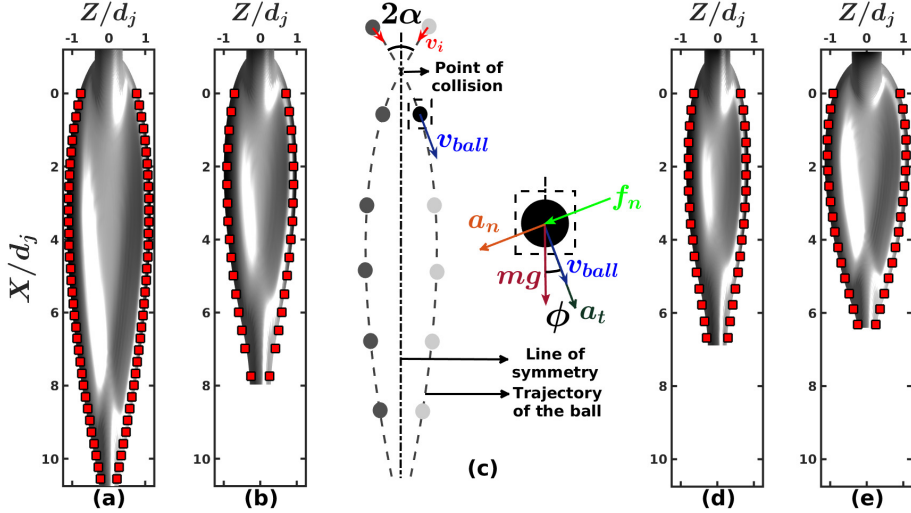


FIGURE 8. Comparison between the link shape and dimension obtained through numerical simulations (iso-surface volume contours) and by using the analytical model using force balance (red colored symbols ■) for different flow configurations (α , Fr , Re/Fr , Bo , e): (a) (), (b) (), (d) () and (e) (), where ϵ is the L^1 relative error norm given by Equation ???. In Figure (c), the schematic of this analytical model is shown.

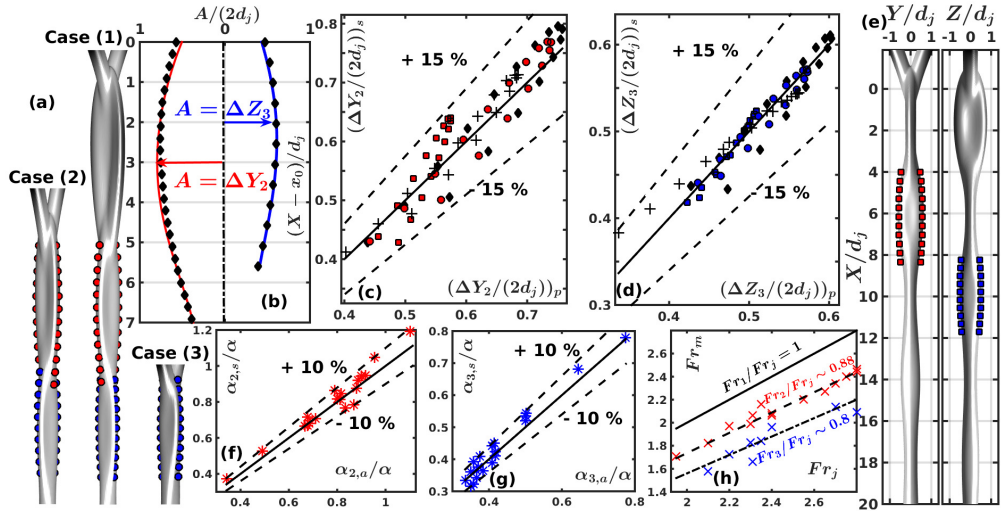


FIGURE 9.

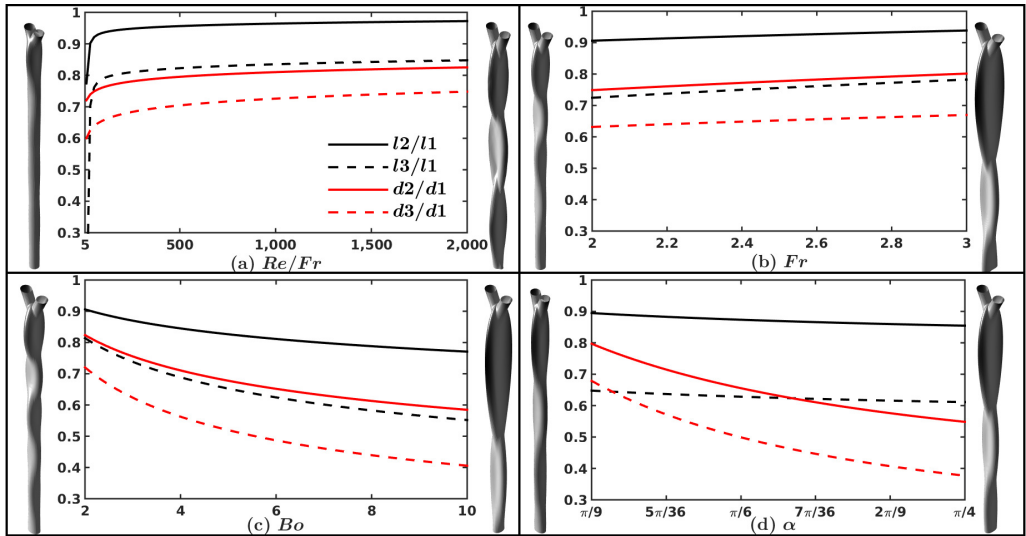


FIGURE 10.

REFERENCES

- BELL, J. B., COLELLA, P. & GLAZ, H. M. 1989 A second-order projection method for the incompressible navier-stokes equations. *Journal of Computational Physics* **85** (2), 257–283.
- BREMOND, N. & VILLERMAUX, E. 2006 Atomization by jet impact. *Journal of Fluid Mechanics* **549**, 273–306.
- BUSH, J. W. M. & HASHA, A. E. 2004 On the collision of laminar jets: fluid chains and fishbones. *Journal of fluid mechanics* **511**, 285–310.
- CHEN, X., MA, D., YANG, V. & POPINET, S. 2013 High-fidelity simulations of impinging jet atomization. *Atomization and Sprays* **23** (12).
- CHOO, Y. J. & KANG, B. S. 2001 Parametric study on impinging-jet liquid sheet thickness distribution using an interferometric method. *Experiments in fluids* **31** (1), 56–62.
- CHOO, Y. J. & KANG, B. S. 2002 The velocity distribution of the liquid sheet formed by two low-speed impinging jets. *Physics of fluids* **14** (2), 622–627.
- CHORIN, A. J. 1968 Numerical solution of the navier-stokes equations. *Mathematics of computation* **22** (104), 745–762.
- DA, F., HAHN, D., BATTY, C., WOJTAN, C. & GRINSPUN, E. 2016 Surface-only liquids. *ACM Transactions on Graphics (TOG)* **35** (4), 78.
- DOMBROWSKI, N. & FRASER, R. P. 1954 A photographic investigation into the disintegration of liquid sheets. *Philosophical Transactions of the Royal Society of London. Series A, Mathematical and Physical Sciences* pp. 101–130.
- EGGERS, J. & VILLERMAUX, E. 2008 Physics of liquid jets. *Reports on progress in physics* **71** (3), 036601.
- ERNI, P. & ELABBADI, A. 2013 Free impinging jet microreactors: controlling reactive flows via surface tension and fluid viscoelasticity. *Langmuir* **29** (25), 7812–7824.
- IBRAHIM, E. A. & PRZEKwas, A. J. 1991 Impinging jets atomization. *Physics of Fluids A: Fluid Dynamics* **3** (12), 2981–2987.
- LING, Y., ZALESKI, S. & SCARDOVELLI, R. 2015 Multiscale simulation of atomization with small droplets represented by a lagrangian point-particle model. *International Journal of Multiphase Flow* **76**, 122–143.
- POPINET, S. 2003 Gerris: a tree-based adaptive solver for the incompressible euler equations in complex geometries. *Journal of Computational Physics* **190** (2), 572–600.
- POPINET, S. 2009 An accurate adaptive solver for surface-tension-driven interfacial flows. *Journal of Computational Physics* **228** (16), 5838–5866.
- RAYLEIGH, LORD 1879 On the capillary phenomena of jets. In *Proc. R. Soc. London*, , vol. 29, pp. 71–97.
- TAYLOR, G. 1960 Formation of thin flat sheets of water. In *Proceedings of the Royal Society of London A: Mathematical, Physical and Engineering Sciences*, , vol. 259, pp. 1–17. The Royal Society.
- VILLERMAUX, E. & CLANET, C. 2002 Life of a flapping liquid sheet. *Journal of fluid mechanics* **462**, 341–363.
- WADHWA, N., VLACHOS, P. & JUNG, S. 2013 Noncoalescence in the oblique collision of fluid jets. *Physical review letters* **110** (12), 124502.
- YANG, L.-J., ZHAO, F., FU, Q.-F. & K.-D.CUI 2014 Liquid sheet formed by impingement of two viscous jets. *Journal of Propulsion and Power* **30** (4), 1016–1026.